Hindawi
Wireless Communications and Mobile Computing
Volume 2023, Article ID 3950769, 19 pages
https://doi.org/10.1155/2023/3950769

Research Article

Miniaturized Ultrawideband Microstrip Antenna for IoT-Based Wireless Body Area Network Applications

Utkarsh Pandey,[1,2] **Parulpreet Singh**,[1] **Raghvendra Singh**,[2] **Narbada Prasad Gupta**,[3] **Sandeep Kumar Arora**,[1] **and Eric Nizeyimana**[4]

[1]*Department of Electronics and Electrical Engineering, Lovely Professional University, Punjab, India*
[2]*Department of Electronics and Electrical, Pranveer Singh Institute of Technology, Kanpur, India*
[3]*JNCT, Bhopal, India*
[4]*College of Science and Technology, University of Rwanda, Rwanda*

Correspondence should be addressed to Parulpreet Singh; parulpreet.23367@lpu.co.in, Sandeep Kumar Arora; sandeep.16930@lpu.co.in, and Eric Nizeyimana; nizerik@yahoo.fr

Received 12 September 2022; Revised 18 February 2023; Accepted 15 March 2023; Published 4 May 2023

Academic Editor: Pietro Manzoni

In this paper, we present an extremely compact ultrawideband (UWB) monopole microstrip patch antenna for a wireless body area network (WBAN). The proposed antenna is fabricated on a flexible Rogers RT-5880 dielectric substrate of thickness 0.5 mm and has an overall size of $20 \times 15 \times 0.5\ mm^3$. The proposed antenna achieves a wideband characteristic with the help of a modified ground plane with a monopole pair. The monopole antenna is fed through a microstrip line and has a good impedance matching over a frequency band of 3.2 to 15 GHz (and beyond), with an axial ratio below 3 dB and a high efficiency of 77–95%. This antenna is designed to cover almost the complete UWB range; bandwidth for antenna is 11.52 GHz (3.48-15 GHz). The antenna has a realized gain of 2.3–7.2 dBi throughout the frequency band and has been tested for conformality. Measured results are found to be in good correlation with the simulated results. The antenna has also been tested for specific absorption rate (SAR) values within the simulation to compare with Federal Communications Commission (FCC) limits and verify their suitability for the Internet of Things- (IoT-) based wearable body area network.

1. Introduction

In recent years, wearable and portable technology has been extensively investigated for their numerous advantages such as serving as a personal digital assistant and providing internet access and multimedia services. Smart watches and rings are examples of wearable technology that are currently being investigated in great depth. These smart devices are equipped with a number of sensors that allow them to communicate wirelessly with other devices, such as a smartphone, as well as with one another. Flexible and textile-based electronics have been in the spotlight for the past decade due to a variety of potential future applications, including wireless tracking, public safety, health monitoring, and other applications [1, 2]. In light of the fact that antennas have an important role in these wearable electronics, wearable and flexible antennas have piqued the interest of several industries working on wireless body area networks (WBANs) [3–5]. People can communicate with one another through the use of wireless body area networks (WBANs), which connect individual nodes placed within clothing or on the skin of a person and extend throughout the human body [4]. Antennas for ultrawideband (UWB) communication systems have a number of additional benefits in addition to their own advantages, such as low power consumption with a limited power spectral density, low cost of implementation, wider channel bandwidth, and higher data transmission rates [6]. Additional considerations

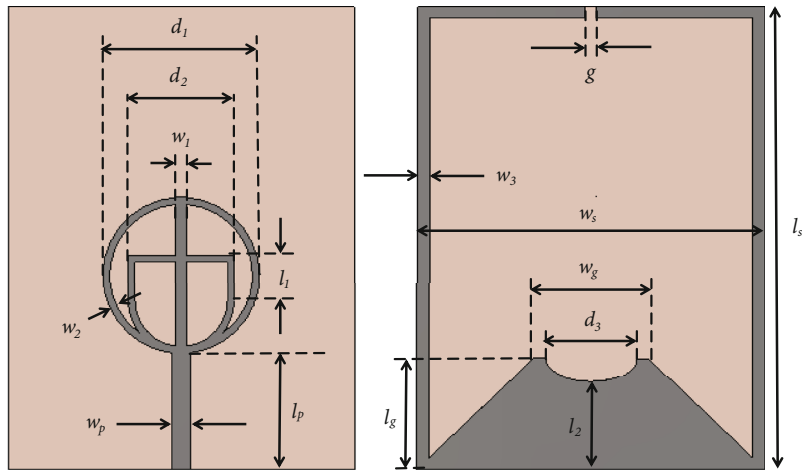

Figure 1: (a) Front and (b) back view of the proposed microstrip monopole antenna designed, dimensions mentioned in Table 1.

include the requirement for circular polarization in the case of body-worn antennas, which is yet another important factor to consider. In many situations, a circularly polarized antenna is preferable to a linearly or elliptically polarized antenna because it aids in the reception of signals regardless of their relative position to the transmitting antenna. As a result, it is more advantageous than a linearly or elliptically polarized antenna. Circular polarization has been achieved using a variety of techniques, including single and double feeds that have been documented in the literature [7]. Single and double feeds have been used to achieve circular polarization. Since the popularity of dual-feed antennas and the ease with which they can be implemented for CP has grown in recent years, several antennas that use a phase shifter [8] and Wilkinson power dividers [9] at the feed have been reported in the literature. The front-end module and control network for the radiator become extremely complex as a result of the simple design of such antennas, making them unsuitable for applications such as WBAN, where compactness is a critical component of the overall system design. An antenna with a single feed circularly polarized radiation pattern is optimal for WBAN applications, which is used in this case [10–14]. In a single feed circularly polarization antenna, the feed port is altered at specific locations in correlation to the feed port, allowing for specific phase shifts, excitation of orthogonal current distribution, and circular polarization. Many different configurations of circular polarized (CP) wideband antennas have been described in the literature [12–16]. In addition to it, having a limited frequency range and a very low gain, such antennas have the disadvantage of requiring complex design in order to achieve a higher gain [17–20]. Using metamaterial-based designs such as complementary split-ring resonators to achieve the desired performance in circularly polarized wideband antennas is another interesting technique for circularly polarized wideband antennas. Such antennas which excite orthogonal surface current for circular polarization and are much larger in size than conventional antennas can be much larger in size.

Table 1: Dimensions of the proposed microstrip monopole antenna (see Figure 1).

Variable	Value (mm)	Variable	Value (mm)
d_1	6.80	w_s	15.00
d_2	4.60	l_s	20.00
d_3	4.00	g	0.50
w_1	0.50	l_1	2.00
w_2	0.30	l_2	2.80
w_3	0.50	l_p	5.00
w_p	0.80	l_g	4.80
w_g	5.00	h	0.50

A number of disadvantages of CP ultrawideband antennas have been identified as a means of circumventing these limitations, including a large form factor to cover UWB, a poor axial ratio, a complex feeding system with dual-feeds, and a high profile with a thicker substrate material, which makes them difficult to use in real-time applications [21–26]. The circularly polarized ultrawideband antenna proposed in this paper can be replaced by a circularly polarized ultracompact ultrawideband antenna, which will overcome the problems mentioned above. The antenna has been demonstrated to operate at frequencies ranging from 3.2 to 15 GHz, and possibly higher frequencies as well. In addition to having a wide gain range (2.3 to 7.4 decibels), it has a high efficiency (more than 70%) across the entire frequency range of operation. An almost perfect isotropic radiation pattern is produced by the antenna, as well as an axial ratio of less than 2.5 dB, which confirms that it is polarized in the circumferential direction. In the design of the presented antenna, we used a K-type 2.4 mm connector to feed the antenna with a coaxial cable. This microstrip line has 50 ohm resistance which is also required in patch antenna design for matching

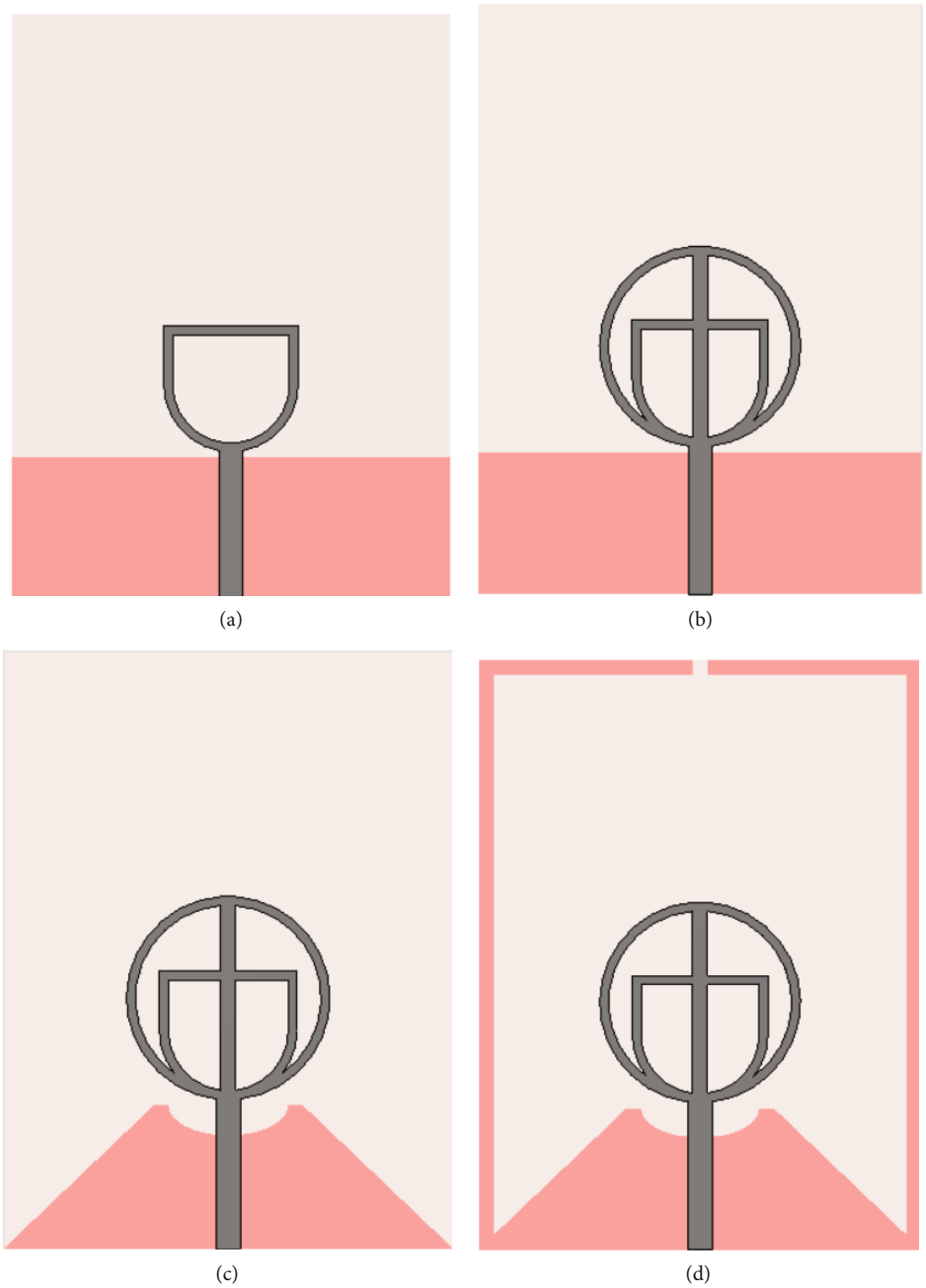

Figure 2: Evolution of the ultrawideband (UWB) antenna: (a) stage I: microstrip line-fed ring-based resonator with a partial ground plane; (b) stage II: concentric ring with a microstrip line vertically passing through the rings; (c) stage III: added notch and triangular cuts on either end in the partial ground plane; and (d) stage IV: monopoles added to the ground plane.

impedance [27–32]. It is demonstrated that the antenna has a very low specific absorption rate (SAR) and that it retains all of its radiation characteristics when in contact with human tissue within the FCC's permitted limits. A low-profile, miniaturized, and conformal antenna must be used when an antenna is placed close to a person's skin. Its operating properties, such as bandwidth, efficiency, gain, and axial ratio, must be in a range which could not harm human skin [33–35]. Wearable antennas are the excellent options for detecting breast cancer; in this, we take care of SAR analysis as well so it has become a boon for the medical industry [36]. The flexible wearable antenna is also convenient for conformality and provides easiness to the person wearing it, in case of a patient that is highly required [37]. There are several techniques for improving the gain of UWB antenna; one of them is frequency selective surface which has been discussed in the literature [38]. One more interesting work of dual-polarized microstrip patch antenna has been presented through literature in which two different antennas are designed on a single chip for different frequency bands, and the optimized design having

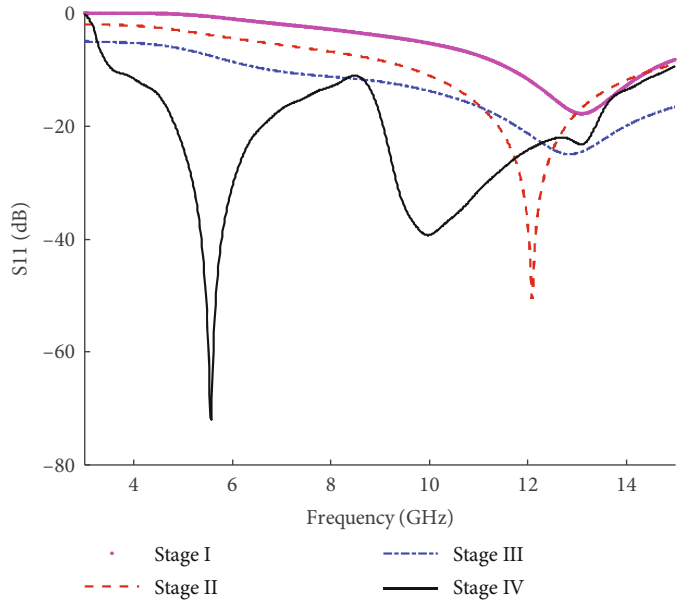

Figure 3: Simulated reflection coefficient (S11) for the proposed antenna and its evolution from stage I to stage IV.

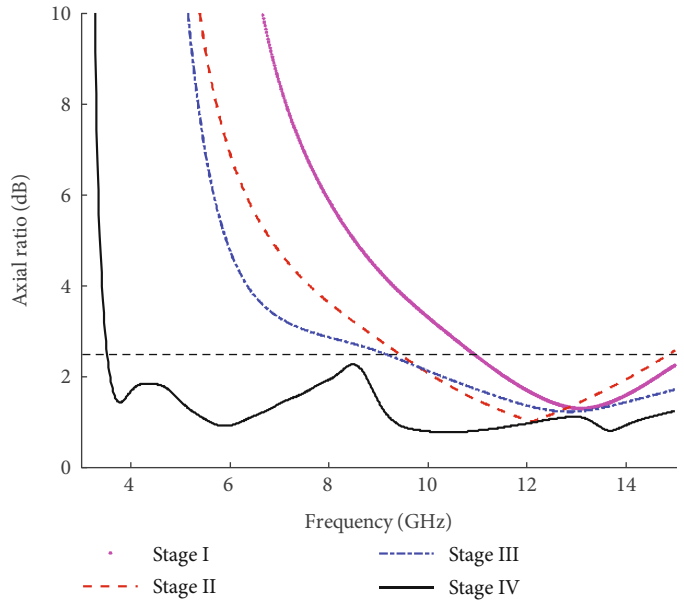

Figure 4: Simulated axial ratio (dB) for the proposed antenna and its evolution from stage I to stage IV.

the two different antenna elements cover the whole UWB [39]. A short sleeve-shaped antenna has been discussed which covers various applications such as 4G LTE services, 5G services, and WiFi services with specific frequency ranges [40]. Listed below is the general structure of the paper: Section 2 deals into the design of the antenna and how it has changed through time. Section 3 presents the results of the simulations and measurements carried out on the proposed antenna, as well as the results of the SAR analysis carried out. The conformity of the antenna and its results of measurements and simulations are presented in Section 4. Section 5 concludes with a succinct summary of the findings presented in Section 4.

2. Antenna Design

2.1. Aspects of Antenna Geometry. As illustrated in Figure 1, the proposed antenna is a microstrip line-fed monopole with a modified ground plane that uses a microstrip line. In order to fabricate the antenna, it is mounted on an RT-5880 dielectric substrate with relative permittivity (ε_r) of 2.2, loss tangent ($\tan\delta$) = 0.0009, and substrate height (h) of 0.5 mm, as shown in the figure. Because of the inherent flexibility of the substrate, it can be stitched with any type of clothing and with minimal effort. The overall size of the antenna is $20 \times 15 \times 0.5\,\text{mm}^3$ ($0.21\,\lambda_0 \times 0.16\,\lambda_0 \times 0.005\,\lambda_0$),

(a) (b)

(c) (d)

Figure 5: Continued.

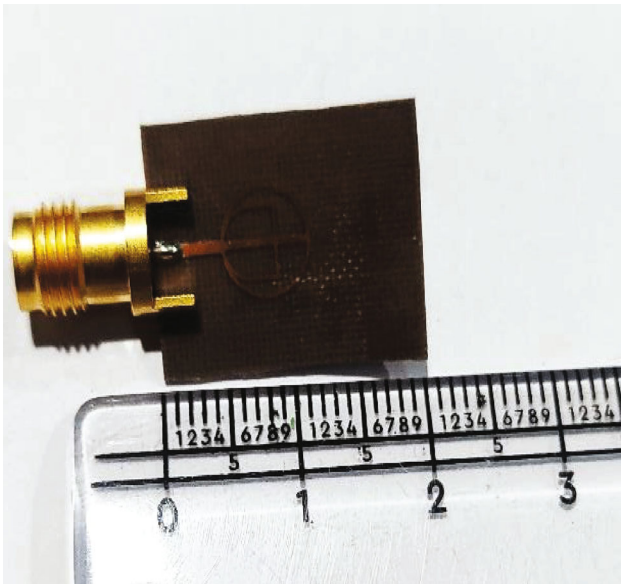

(e)

Figure 5: (a) Front view, (b) back view, (c) conformal fabricated antenna, (d) width representation of fabricated antenna, and (e) length representation of fabricated antenna.

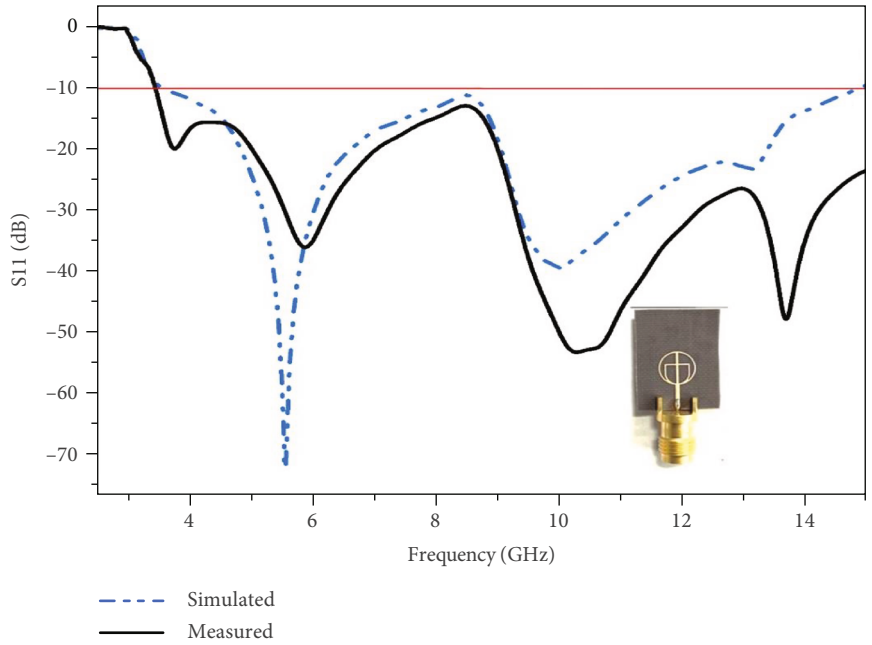

Figure 6: Measured and simulated *S*-parameters for the proposed UWB monopole antenna.

where λ_0 is the cut-off wavelength for the antenna and λ_0 is equivalent to 3.2 GHz. Table 1 shows the antenna's dimensions in millimeters. A 50 microstrip line fed with a discrete port was used in the simulation; however, in the actual fabricated antenna, a 2.4 mm K-type connector was used instead of the previously mentioned discrete port.

2.2. Evolution of the Antenna. In Figure 2, it can be observed how the proposed antenna has evolved from its inception to its current state over the course of the years since it was first proposed. It is simple to understand and put into practice the antenna design that is proposed, which starts with a ring resonator and partial ground plane configuration. When the impedance match is incorrect, as shown in Figure 2(a), stage I can produce a frequency band between 10 and 15 GHz, which is indicative of a bad impedance match. In order to complete stage II of the design, it was necessary to incorporate a concentric ring as well as a microstrip line that ran vertically

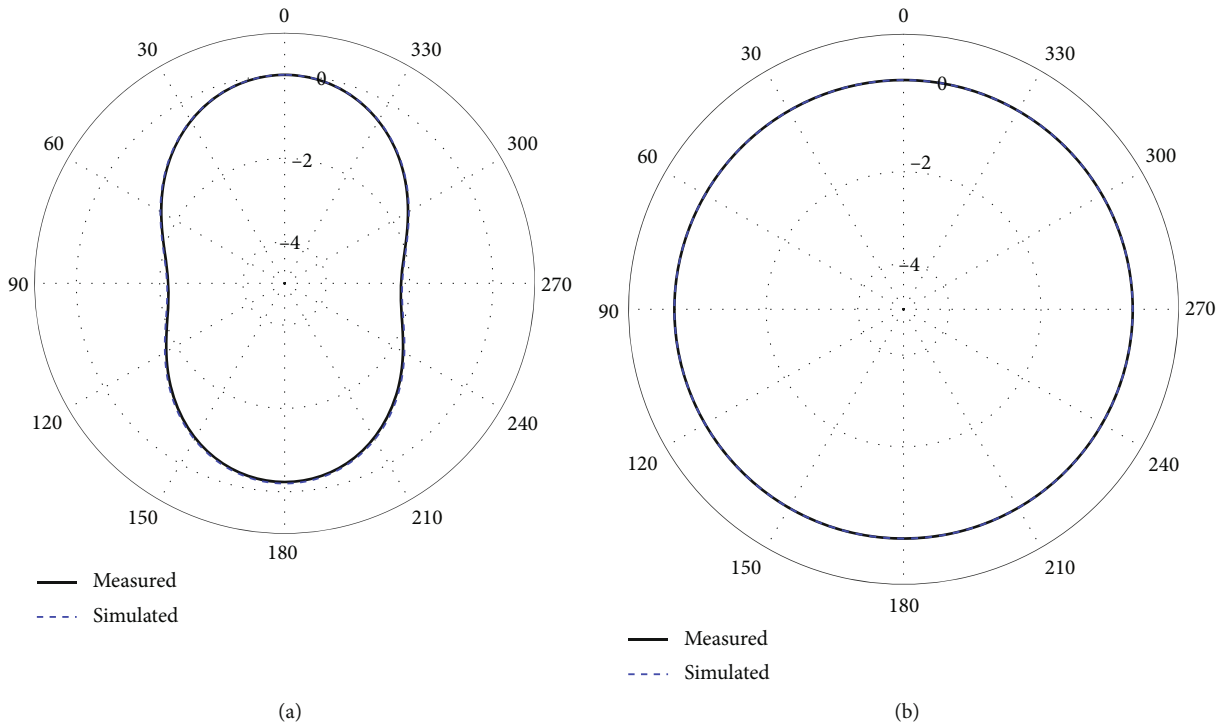

Figure 7: Measured and simulated normalized radiation pattern at 4 GHz in (a) azimuth and (b) elevation plane.

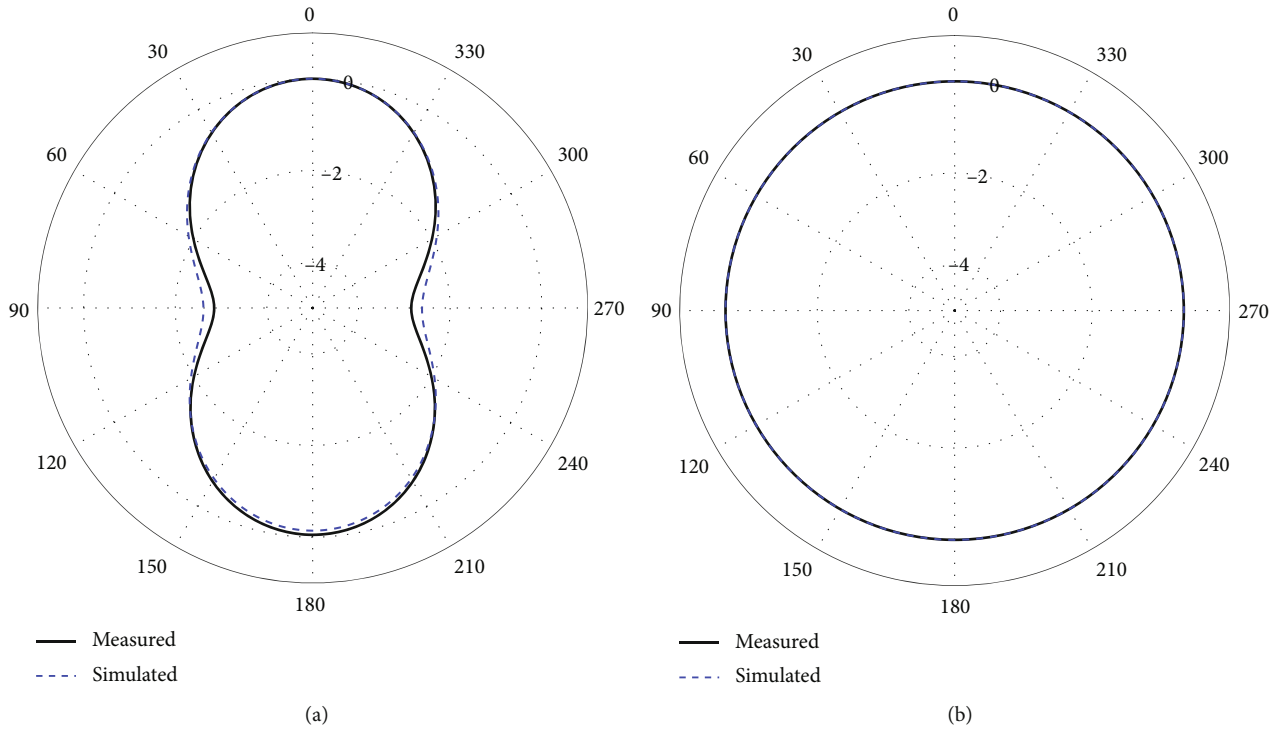

Figure 8: Measured and simulated normalized radiation pattern at 8 GHz in (a) azimuth and (b) elevation plane.

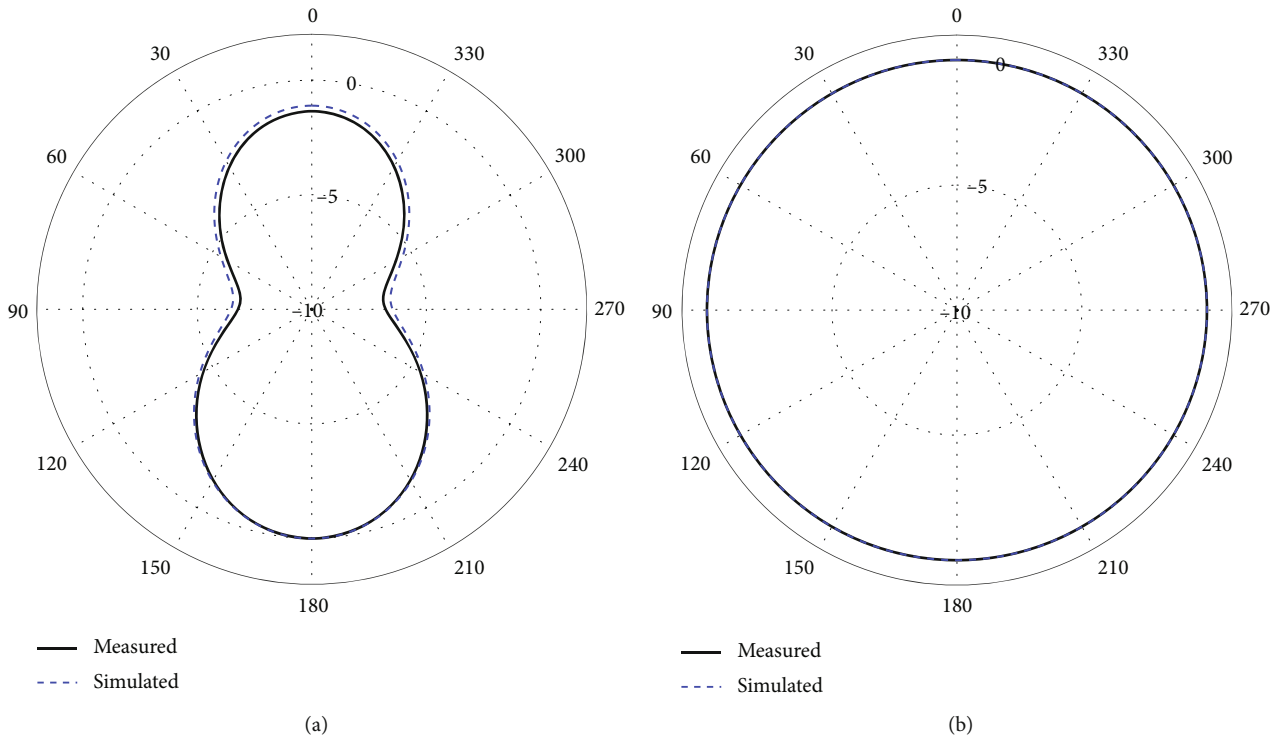

Figure 9: Measured and simulated normalized radiation pattern at 11 GHz in (a) azimuth and (b) elevation plane.

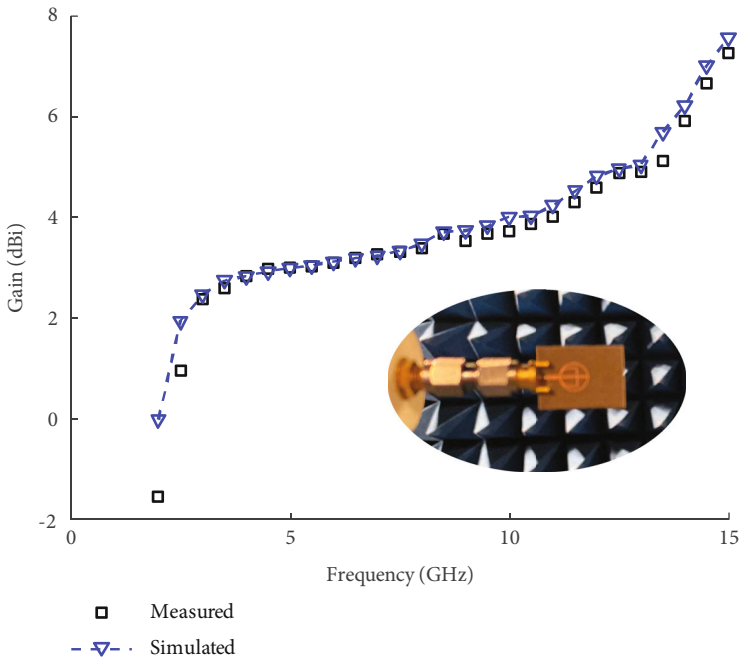

Figure 10: Simulated and measured gain for the proposed antenna.

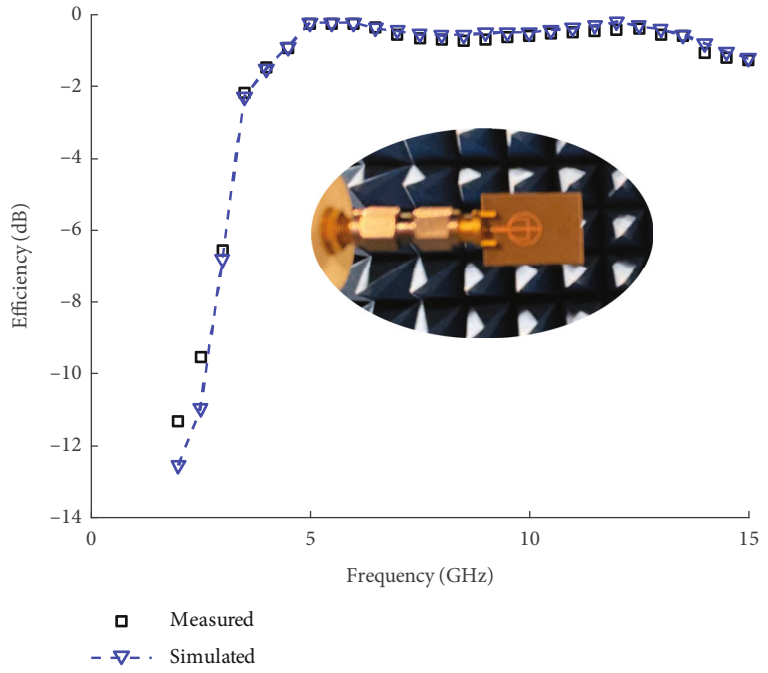

Figure 11: Simulated and measured efficiency of the proposed antenna.

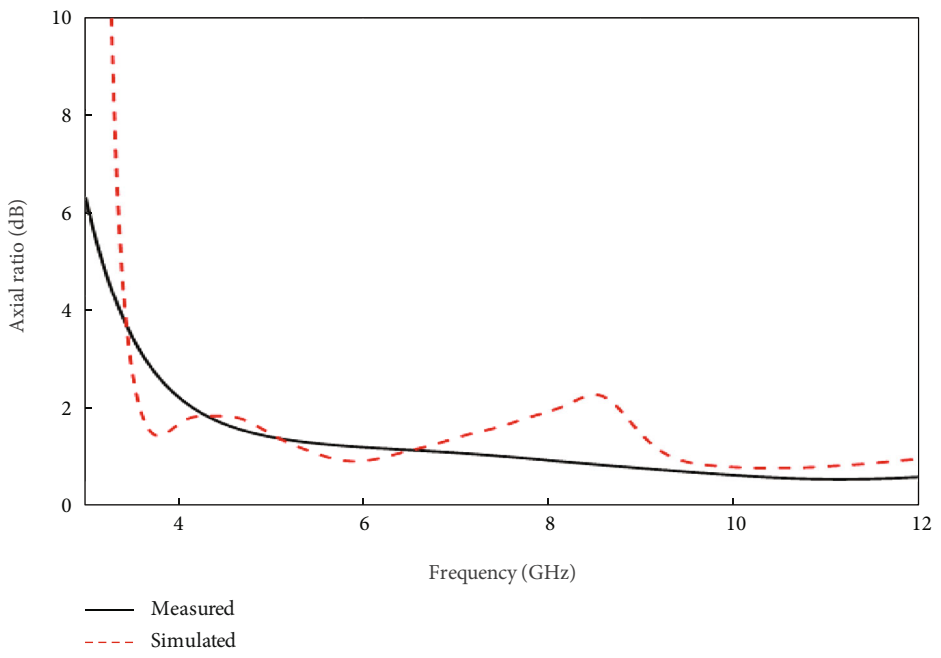

Figure 12: Measured and simulated axial ratio for the proposed antenna.

through the radiating monopole, as shown in Figure 2(b). There is a shift in the frequency bands in this case, from 8 to 15 GHz, and circular polarization is used in the band of 8.5 to 15 GHz, while linear polarization is used in the rest of the bands. The antenna's frequency bands have been expanded to include 8–15 GHz. The partial ground plane is modified at the conclusion of stage III by cutting a notch in the middle and making triangular cuts at both ends of the ground plane. It is possible to increase the frequency range to 6–15 GHz while maintaining symmetry (see Figure 2(c)), with circular polarization for frequencies 6.5–15 GHz and linear polarization for the remaining frequencies.

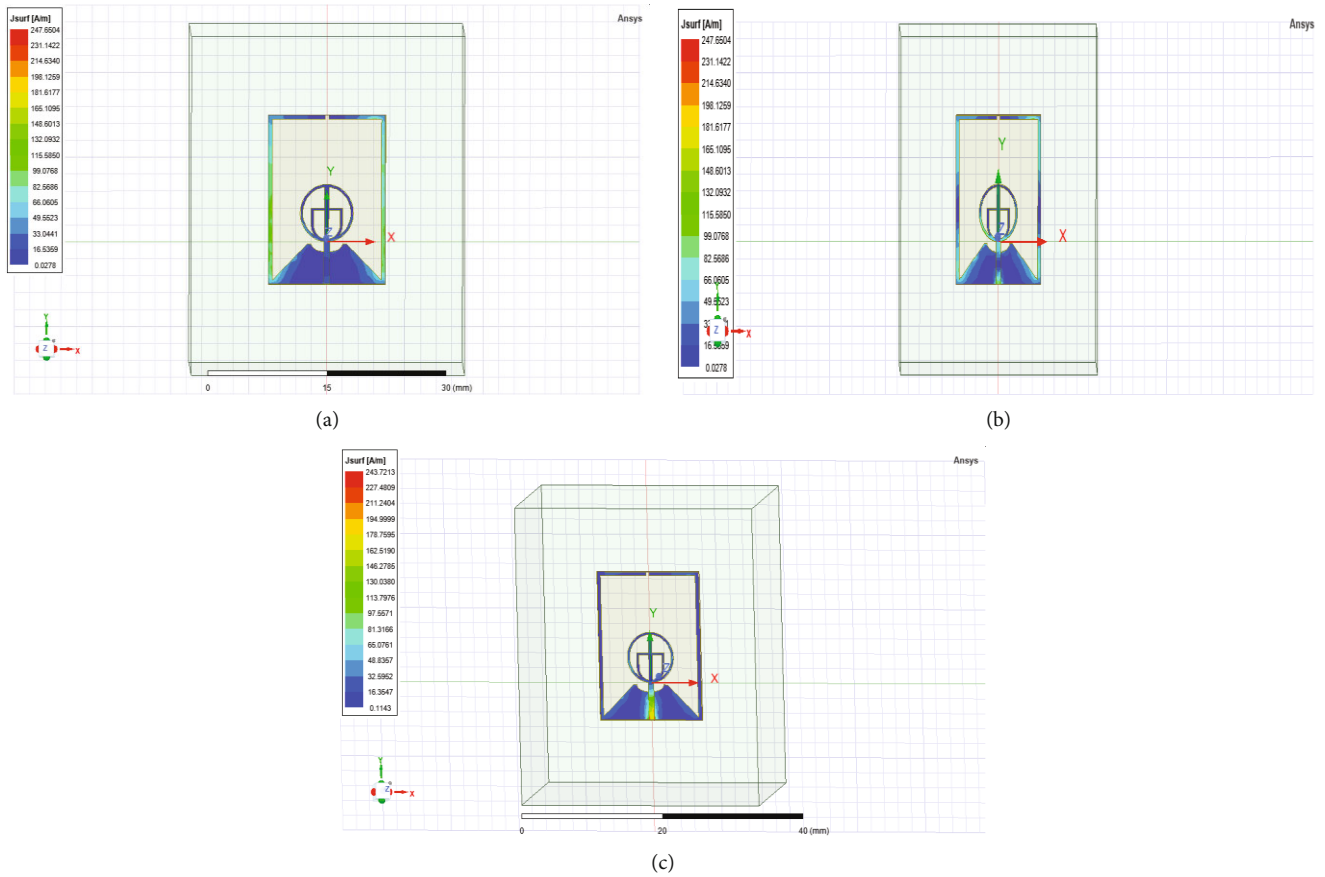

FIGURE 13: (a) Surface current distribution at 4 GHz. (b) Surface current distribution at 8 GHz. (c) Surface current distribution at 11 GHz.

Figure 2 depicts an illustration of the final stage (stage IV) of the process. Essentially, it is made up of two monopole microstrip lines separated by an equal width gap ($g = 0.25$ mm) at the ground plane on either side of the ground plane (d). It is possible to maintain axial ratios of less than 3 dB throughout the frequency range of the final antenna, which operates in the range of 3.2 to 15 GHz for the duration of the antenna's operation. The cuts in the ground plane help in achieving the appropriate return loss in the 8–10 GHz frequency band. The simulated results for S-parameters and axial ratio are shown in Figures 3 and 4, respectively, as are the simulated results for the same parameters. This has resulted in the determination that the antenna has been circularly polarized due to its simulation having an effective axial ratio of 2.5 dB.

3. Measured Results

3.1. Fabricated Design. The proposed antenna has been fabricated using the general photolithography process and is shown in Figure 5. Figure 5(a) represents the front view of the fabricated antenna while Figure 5(b) denotes the back of the fabricated antenna. Similarly, Figures 5(c)–5(e) denote the conformality, width, and length of the fabricated antenna. The antenna is fabricated on a Rogers RT-5880 dielectric substrate of relative permittivity, $\varepsilon_r = 2.2$ and loss tangent, $\tan\delta = 0.0009$. It uses a K-type 2.4 mm connector to feed the antenna with a coaxial cable; this connector is having 50 ohm resistance.

Figure 6 depicts the reflection coefficients of the proposed antenna based on simulations and measurements, respectively. The antenna exhibits a -10 dB frequency range of 3.48 GHz to 15 GHz (and beyond), with a fractional bandwidth of 124.67 percent of the center frequency (it was not the fractional bandwidth but as per suggestion when I went through the standard papers, it is also an important parameter to find out so it is 124.68%).

$$\text{Impedance } BW = \frac{15 - 3 \cdot 48}{9 \cdot 24} \times 100. \quad (1)$$

Here, 9.24 is the center frequency. That can be found out as $(3.48 + (15 - 3.48/2)) = 9.24$.

The S-parameter of the measured antenna is in excellent agreement with the simulated results, indicating that the measurements were accurate. The slight difference in S11 at 13 GHz and beyond is believed to be because of human errors during the manufacturing process.

3.2. Radiation Characteristics. The antenna was tested in an anechoic chamber with an NSI2000 system. Figures 7–9

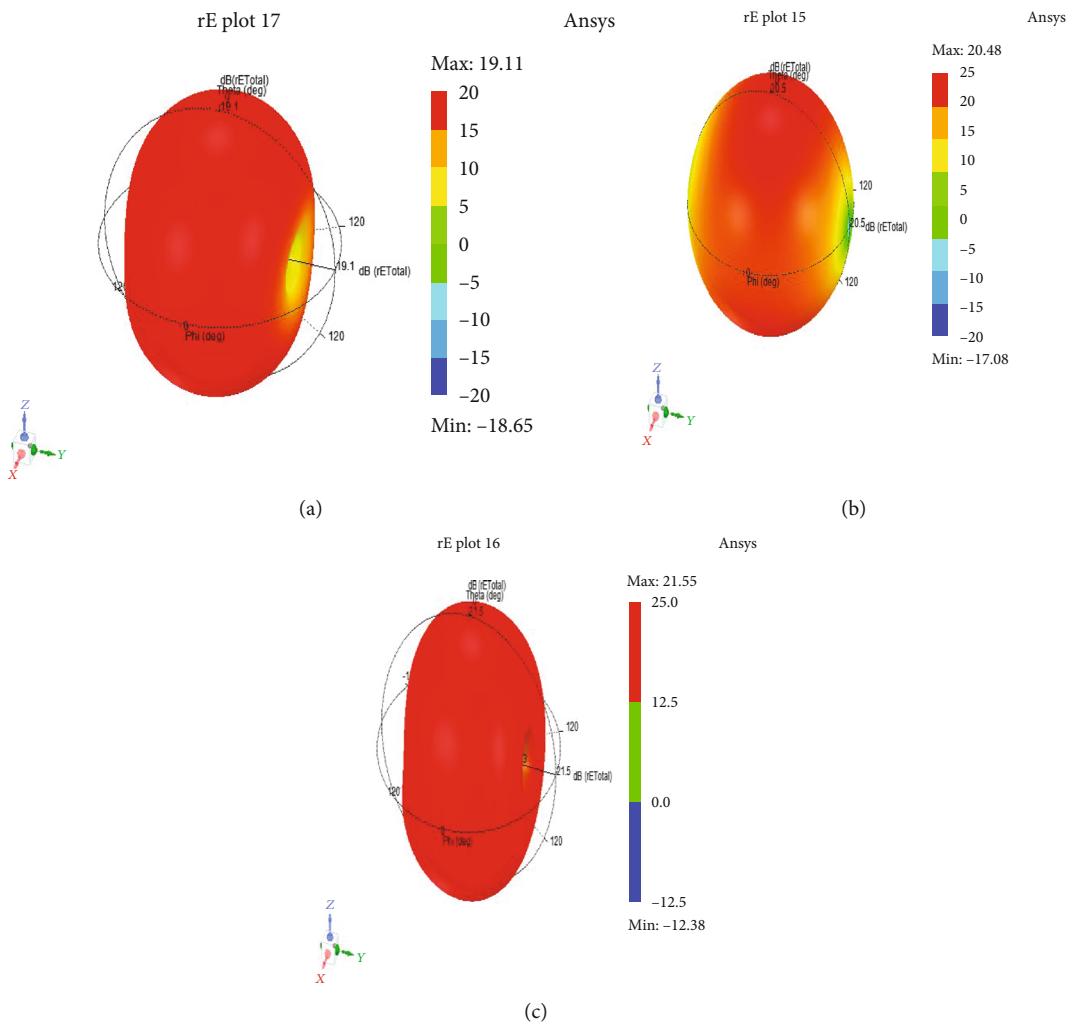

Figure 14: 3D polar plot for (a) 4 GHz. (b) 3D polar plot for 8 GHz. (c) 3D polar plot for 11 GHz.

depict the measured and simulated radiation patterns of the antennas in the azimuth and elevation planes at 4 GHz, 7 GHz, and 11 GHz, normalized to 0 dB, for the three different frequency bands studied. Because the patterns observed and predicted by the simulation are very similar, the antenna exhibits an almost perfect monopole characteristic.

According to the results of the measurements, the antenna has an average gain of 2.44 to 7.22 decibels and a total efficiency of more than 77 percent throughout the operating frequency band. Figures 10 and 11 show the comparison of the measured gain and total efficiency with the simulated results, and both show a very good agreement with the simulated results. Figure 10 shows the comparison of the measured gain with the simulated results.

The cross-polarized results for the antenna are found to be very similar to copolarized results in both simulation and measurement and hence are not included here for brevity. Hence, it can be said with confidence that the antenna is circularly polarized. Further, the measured axial ratio below 3 dB shown in Figure 12 for the antenna confirms the circularly polarized nature of the antenna.

Figures 13(a)–13(c) show the surface current distribution at 4 GHz, 8 GHz, and 11 GHz. It can be observed through the figures that the current distribution is uniform over circular patch and ground. Figures 14(a)–14(c) show 3D polar plot of radiation pattern for different frequencies as mentioned below each pattern. Figures 15(a)–15(c) represent vector surface current distribution [27].

When an antenna system radiates electromagnetic waves, it is possible that these waves will penetrate human tissue and cause harm to the human body. It is possible to determine the nature of these emissions as well as their impact on the human body by measuring the specific absorption rate (SAR). SAR is a unit of measurement for the amount of power dissipated per unit of mass. The FCC (Federal Communications Commission) has established SAR limits of a maximum of 2 W/kg for 10 g of tissue, with a lower limit of 1 W/kg for 10 g of tissue as the upper and lower limits, respectively. Using CST Microwave Studio, the SAR was calculated, and the antenna's placement in relation to the human body model is depicted in Figure 16 [33]. Table 2, which is a graphical representation of the electrical

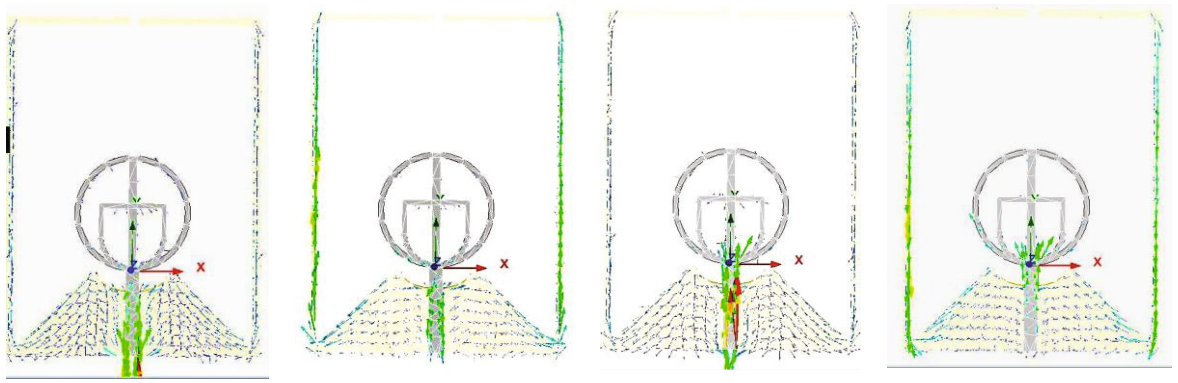

(a) (b) (c) (d)

Figure 15: Surface current distributions at f (4.0 GHz) with different phases, (a) 0°, (b) 90°, (c) 180°, and (d) 270°.

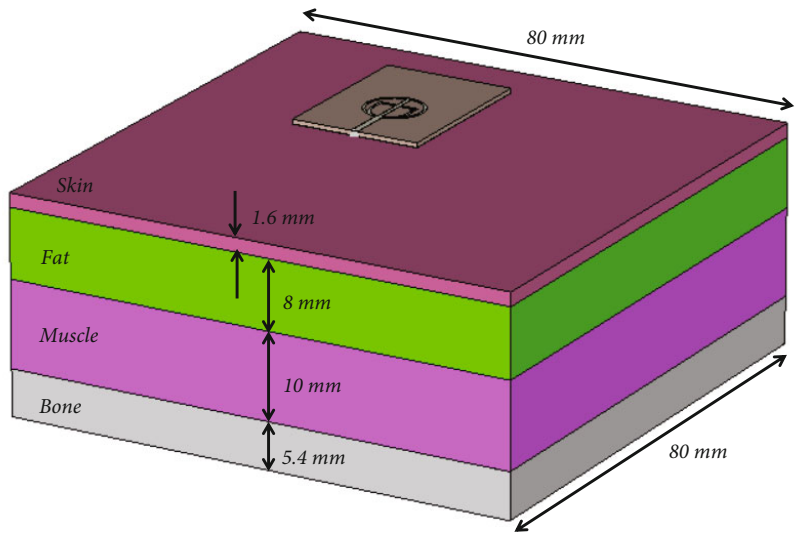

Figure 16: Antenna placed on a human body model within CST Microwave Studio [33].

Table 2: Electrical properties of the human body model at 4 GHz.

Layer	Relative permittivity εr	Conductivity σ (S/m)	Density (kg/m3)	Thickness (mm)
Skin	41.4	1.49	1001	1.6
Fat	5.46	0.11	900	8
Muscle	55	1.77	1006	10
Bone	18.5	0.82	1008	5.4

properties of the human body model, describes the electrical properties of the model.

The antenna is placed at a distance of 5 mm from the human body to simulate an approximate real-life situation with an input power of 0.5 mW to meet the standards defined for SAR measurement. The SAR simulation for 4, 7, 9, and 11 GHz are shown in Figure 17.

The antenna has the highest SAR of 1.82 W/kg at 3.5 GHz, and it reduces down to 0.84 W/kg at 11 GHz, and 0.63 W/kg at 15 GHz, see Figure 16. This simulated SAR is way below the FCC limits and hence makes the proposed antenna suitable for wireless body area networks (WBANs) and for wearable electronics.

4. Conformal Antenna

A thin substrate with a height of 0.5 mm has been used in the design of the proposed antenna; as a result, the antenna can be bent to a specific radius with relative ease. However, due to the extremely small size of the antenna, it is difficult to bend it past a certain point. As shown in this section, the antenna was conformed to a radius of 50 mm, and the

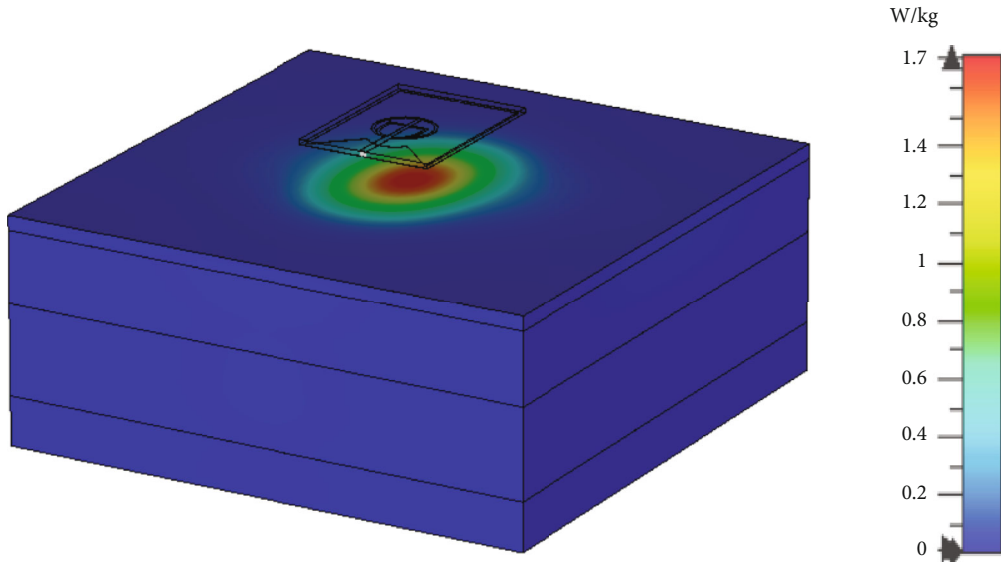

(a)

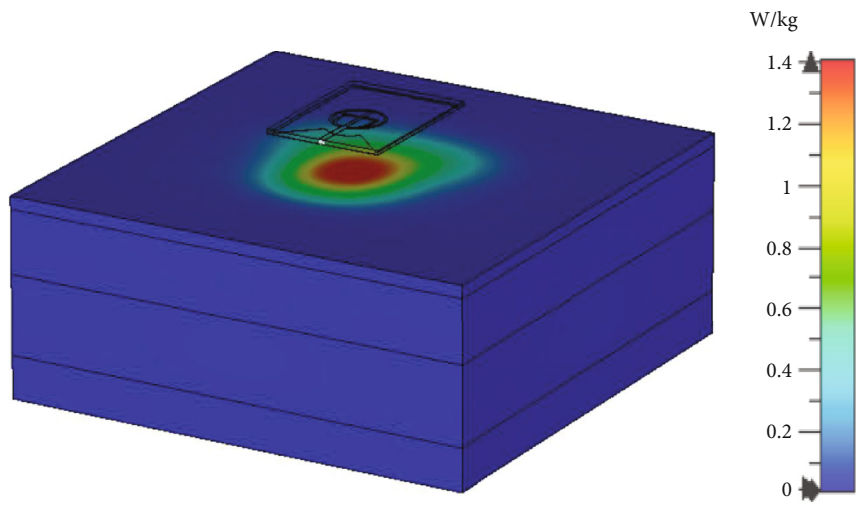

(b)

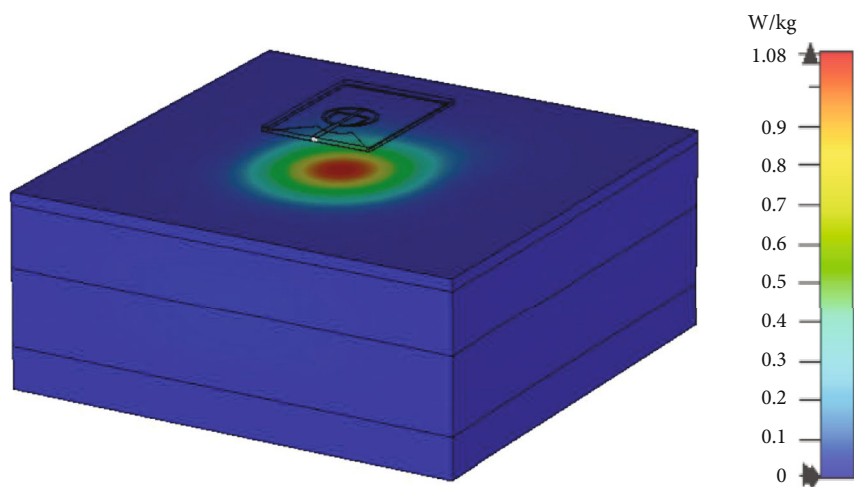

(c)

Figure 17: Continued.

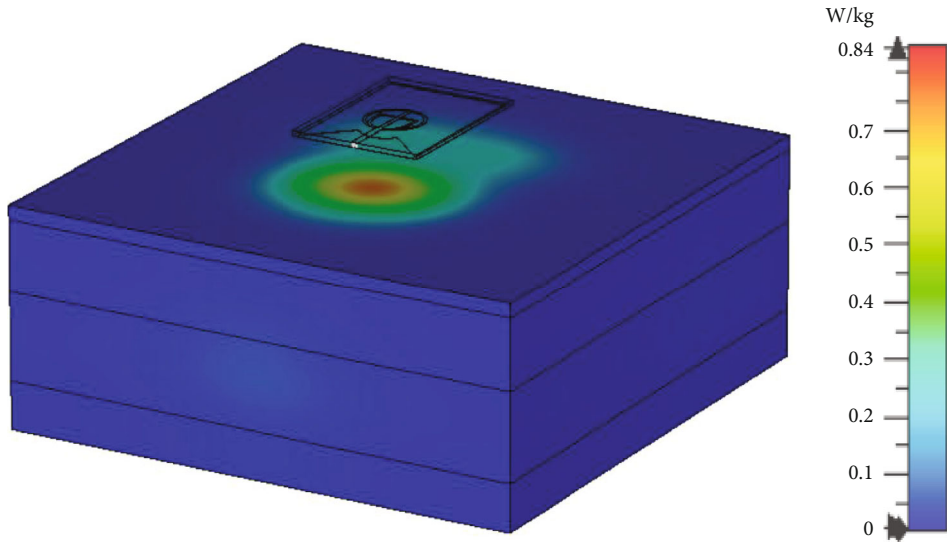

(d)

Figure 17: Simulated SAR analysis at (a) 4 GHz, (b) 7 GHz, (c) 9 GHz, and (d) 11 GHz.

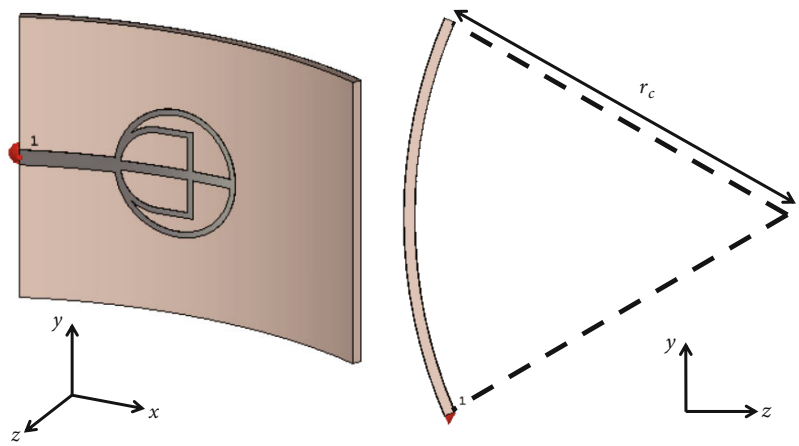

(a) (b)

Figure 18: (a) 3D view and (b) YZ-plane of the conformal antenna of radius $r_c = 50$ mm.

measured results were discussed and compared to those obtained with flat antennas. The conformed design that was simulated in CST-MWS is depicted in Figure 18.

The measured S11 for the conformal antenna, compared with the normal antenna is shown in Figure 19. The antenna shows a similar reflection coefficient as the normal antenna and hence provides the same 3.2–15 GHz (and beyond). The slight difference in the S-parameters is believed to be because of the minute capacitance being generated with metallic layers being brought closer with the bend, which further affects the surface current. The measured normalized radiation pattern compared with the normal antenna for 3, 7, and 11 GHz is shown in Figures 20–22.

When the normalized measured radiation pattern for the conformal antenna is compared to the planar antenna, it is discovered to be approximately similar. In Figure 23, it can be seen that while the gain of the conformal antenna is very similar to that of the normal antenna, there is only a small difference of 0.2 dB between the two, where the conformal antenna has a slightly lower gain. This is expected as the bend in the antenna affects the antenna aperture and hence reduces the gain. The total efficiency of the conformal antenna follows the same trend as that of the normal antenna, as depicted in Figure 24. Please note that the conformity of the antenna was only tested in YZ-plane and not in XZ-plane. This is because of the size of the antenna and the type of material. The dimension of the antenna being much smaller in the XZ-plane was not possible to physically bend the material in measurement, and hence, the conformal results for the same have not been included.

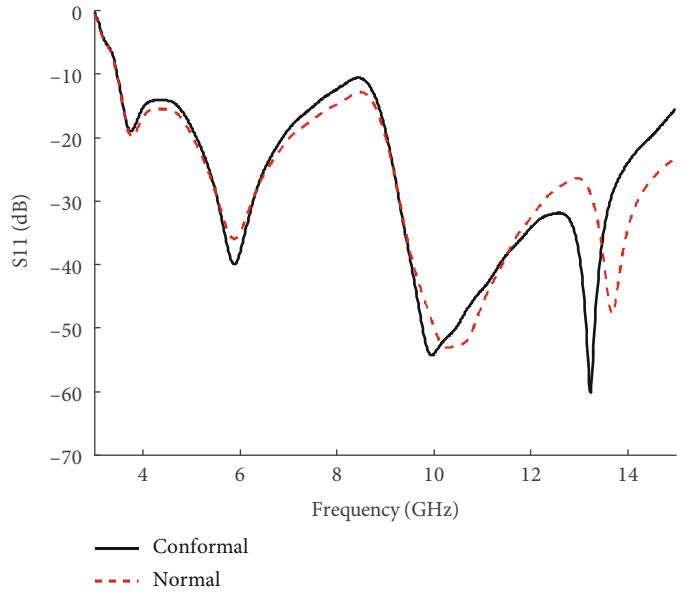

Figure 19: Measured reflection coefficient for the conformal antenna ($r_c = 50$ mm) compared with the normal antenna.

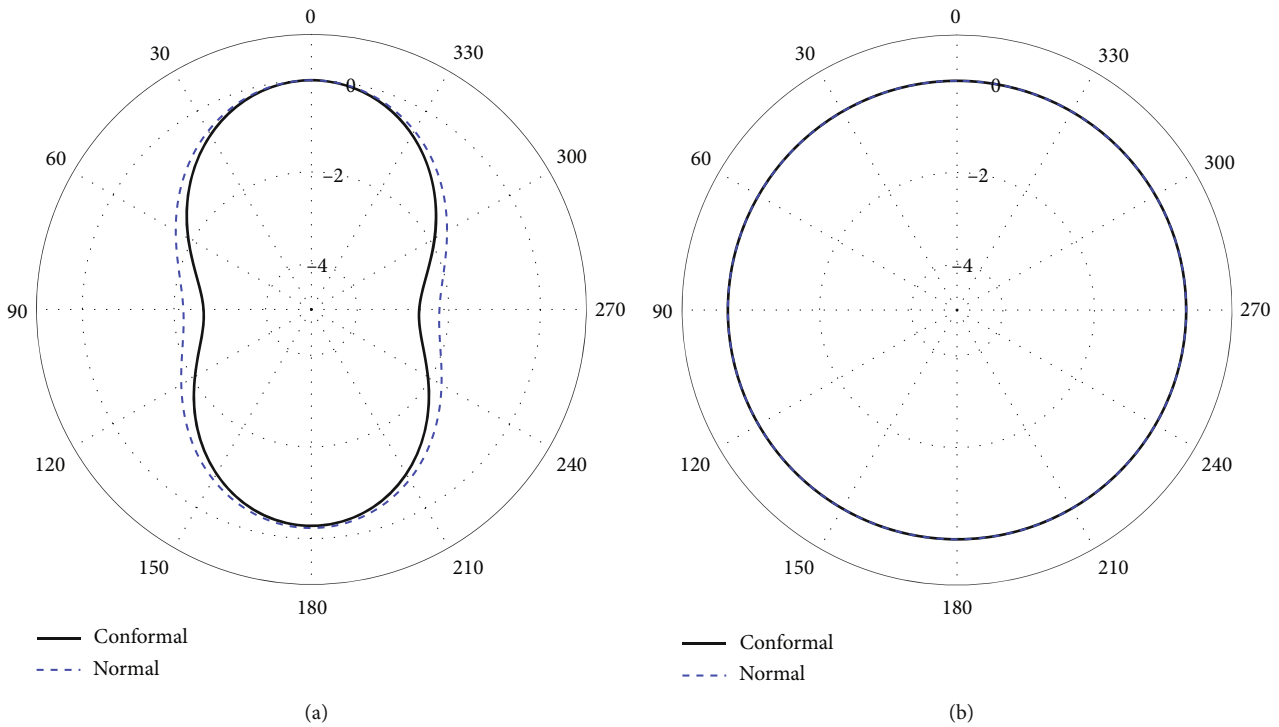

Figure 20: Measured and simulated normalized radiation pattern at 4 GHz in (a) azimuth and (b) elevation plane.

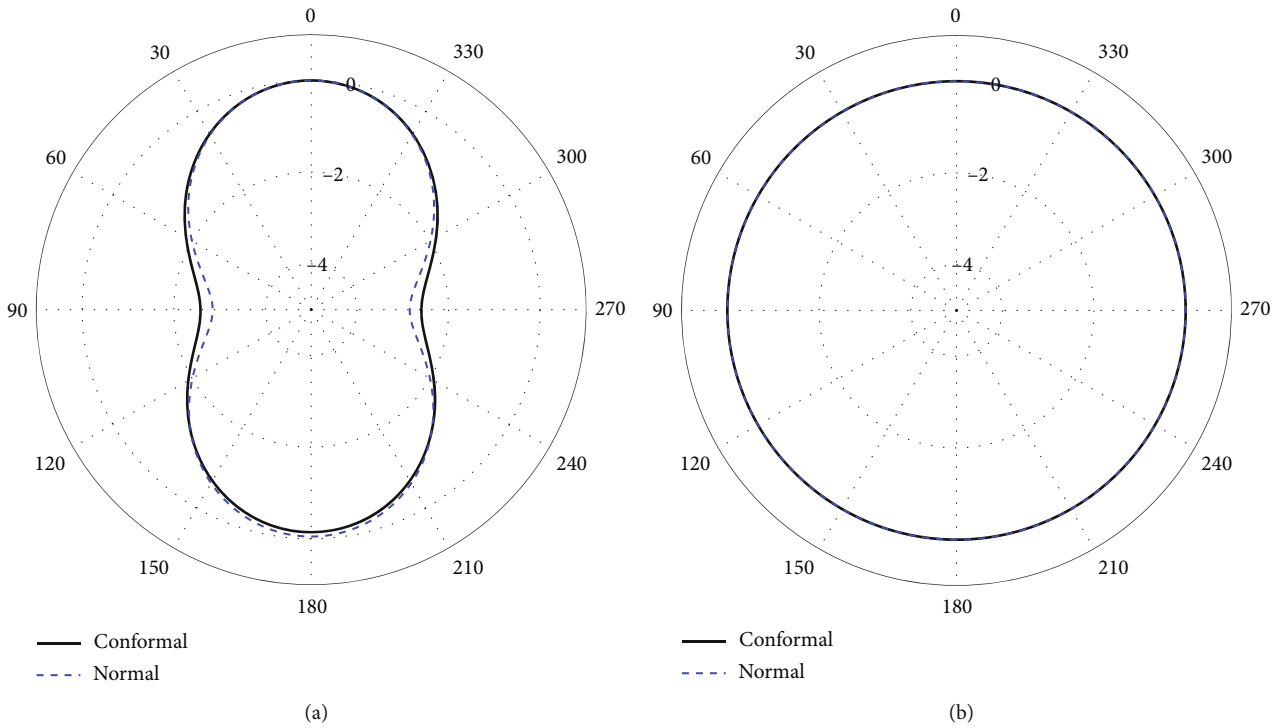

Figure 21: Measured and simulated normalized radiation pattern at 7 GHz in (a) azimuth and (b) elevation plane.

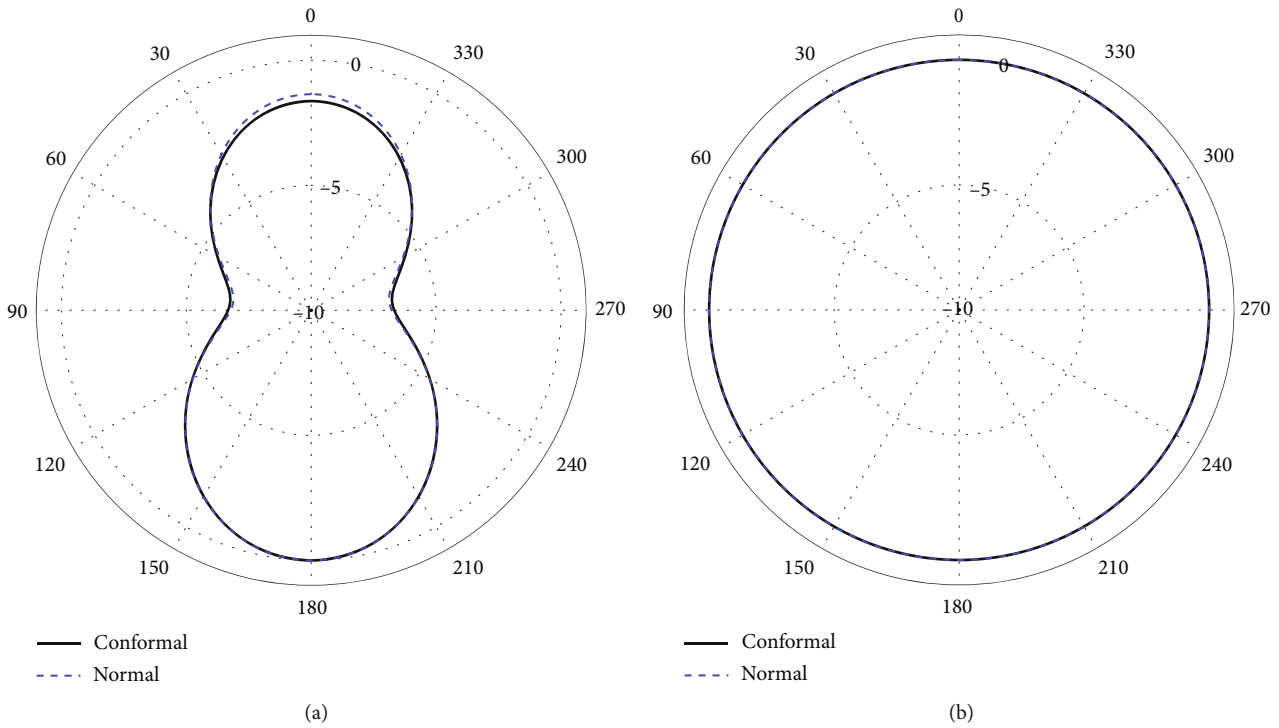

Figure 22: Measured and simulated normalized radiation pattern at 11 GHz in (a) azimuth and (b) elevation plane.

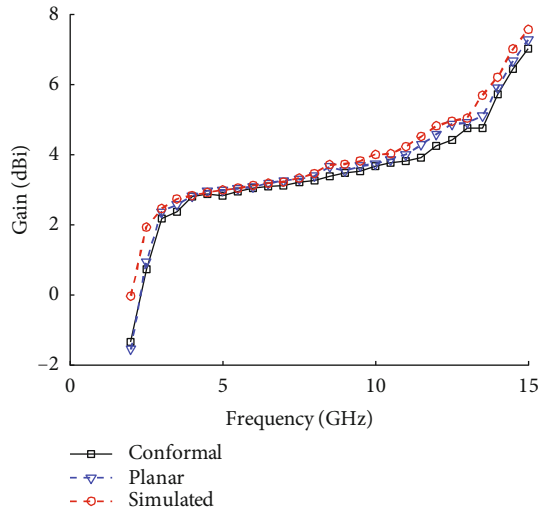

Figure 23: Measured gain for the conformal and planar antenna, compared with the simulated antenna.

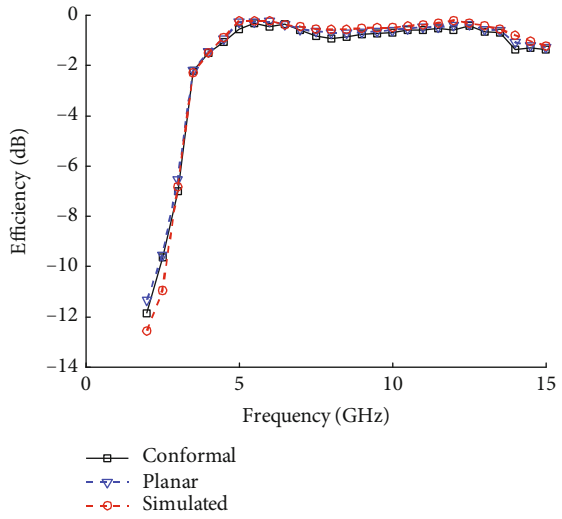

Figure 24: Measured total efficiency for the conformal and planar antenna, compared with the simulated antenna.

Table 3: Comparing the proposed antenna with the literature.

Ref	Size (mm^3)	Freq (GHz)	Axial ratio BW (GHz)	Gain (dBi)	Efficiency (%)
[9]	$66 \times 80 \times 1$	2–10	3.2–6.1	1.6	80–85
[12]	$44 \times 44 \times 1.6$	2.25–4	2.4–4	3–3.5	>85
[13]	$101 \times 64 \times 1.54$	3.6–9.2	4.2–9.1	3.9–7.3	—
[16]	$60 \times 40 \times 1$	1.9–10.6	3.7–10.6	3–4.8	—
[41]	$25 \times 25 \times 1$	8.4–15.2	9.8–13	4.1	>72
[34]	$120 \times 120 \times 0.8$	2–7	2–6	8–12 (antenna being a 2×2 array)	—
[42]	$90 \times 90 \times 4.2$	1.5–7	2.2–7	5–13 (antenna being a 2×2 array)	91
[43]	$36 \times 30 \times 1.5$	2.9–12	—	1.2–6.3	85
This work	$20 \times 15 \times 0.5$	3.48–15	3.48–9	2.5–7.5	77–93

5. Conclusion

This research proposes a circularly polarized ultrawideband (UWB) monopole antenna for use in wearable body area networks (WBANs). In order to build the radiator, we used a microstrip feed and a simple concentric ring-based design. In order to achieve this, an altered concentric ring radiator and an altered ground plane have been used in tandem. An axial ratio of less than 2.5 dB is maintained across the whole bandwidth of the proposed antenna. When it comes to transmitting, the antenna is extremely efficient. For wearable applications, the antenna's 10 g SAR analysis shows that it falls well inside the FCC's limit. Table 3 compares the suggested antenna to other similar antennas that have been previously published in the literature, allowing the reader to better comprehend the novelty of the proposed research.

Data Availability

The data will be available on request.

Conflicts of Interest

The authors declare that there are no conflicts of interest.

References

[1] S. Sankaralingam and B. Gupta, "Development of textile antennas for body wearable applications and investigations on their performance under bent conditions," *Progress In Electromagnetics Research B*, vol. 22, pp. 53–71, 2010.

[2] M. E. B. Jalil, M. K. Abd Rahim, N. A. Samsuri et al., "Fractal Koch multiband textile antenna performance with bending, wet conditions and on the human body," *Progress In Electromagnetics Research*, vol. 140, pp. 633–652, 2013.

[3] S. N. Mahmood, A. J. Ishak, T. Saeidi et al., "Recent advances in wearable antenna technologies: a review," *Progress In Electromagnetics Research B*, vol. 89, pp. 1–27, 2020.

[4] S. N. Mahmood, A. J. Ishak, A. Ismail, A. C. Soh, Z. Zakaria, and S. Alani, "ON-OFF body ultra-wideband (UWB) antenna for wireless body area networks (WBAN): a review," *IEEE Access*, vol. 8, pp. 150844–150863, 2020.

[5] A. Bansal and R. Gupta, "A review on microstrip patch antenna and feeding techniques," *International Journal of Information Technology*, vol. 12, no. 1, pp. 149–154, 2020.

[6] P. B. Samal, P. J. Soh, and G. A. E. Vandenbosch, "UWB all-textile antenna with full ground plane for off-body WBAN communications," *IEEE Transactions on Antennas and Propagation*, vol. 62, no. 1, pp. 102–108, 2014.

[7] Y. F. Lin, H. M. Chen, F. H. Chu, and S. C. Pan, "Bidirectional radiated circularly polarised square-ring antenna for portable RFID reader," *Electronics Letters*, vol. 44, no. 24, pp. 1383-1384, 2008.

[8] J. Y. Jan, C. Y. Pan, K. Y. Chiu, and H. M. Chen, "Broadband CPWfed circularly-polarized slot antenna with an open slot," *IEEE Transactions on Antennas and Propagation*, vol. 61, no. 3, pp. 1418–1422, 2013.

[9] A. Narbudowicz, M. John, V. Sipal, X. Bao, and M. J. Ammann, "Design method for wideband circularly polarized slot antennas," *IEEE Transactions on Antennas and Propagation*, vol. 63, no. 10, pp. 4271–4279, 2015.

[10] H. H. Tran, N. Nguyen-Trong, and A. M. Abbosh, "Simple design procedure of a broadband circularly polarized slot monopole antenna assisted by characteristic mode analysis," *IEEE Access*, vol. 6, pp. 78386–78393, 2018.

[11] J. Wei, X. Jiang, and L. Peng, "Ultrawideband and high-gain circularly polarized antenna with double-Y-shape slot," *IEEE Antennas and Wireless Propagation Letters*, vol. 16, pp. 1508–1511, 2017.

[12] K. Ding, C. Gao, T. Yu, and D. Qu, "Broadband C-shaped circularly polarized monopole antenna," *IEEE Transactions on Antennas and Propagation*, vol. 63, no. 2, pp. 785–790, 2015.

[13] T. T. Le, H. H. Tran, and H. C. Park, "Simple-structured dual-slot broadband circularly polarized antenna," *IEEE Antennas and Wireless Propagation Letters*, vol. 17, no. 3, pp. 476–479, 2018.

[14] R. Gupta, G. Bakshi, and A. Bansal, "Dual-band circularly polarized stacked sapphire and TMM13i rectangular DRA," *Progress In Electromagnetics Research M*, vol. 91, pp. 143–153, 2020.

[15] U. Ullah and S. Koziel, "A geometrically simple compact wideband circularly polarized antenna," *IEEE Antennas and Wireless Propagation Letters*, vol. 18, no. 6, pp. 1179–1183, 2019.

[16] R. Xu, J. Y. Li, K. Wei, and G. W. Yang, "Broadband rotational symmetry circularly polarised antenna," *Electronics Letters*, vol. 52, no. 6, pp. 414–416, 2016.

[17] X. Ren, S. Liao, and Q. Xue, "Design of wideband circularly polarized Vivaldi antenna with stable radiation pattern," *IEEE Access*, vol. 6, pp. 637–644, 2018.

[18] M. S. Ghaffarian, G. Moradi, and P. Mousavi, "Wide-b-and circularly polarised slot antenna by using artificial transmission line," *IET Microwaves, Antennas & Propagation*, vol. 11, no. 5, pp. 672–679, 2017.

[19] Y.-W. Zhong, G.-M. Yang, J.-Y. Mo, and L.-R. Zheng, "Compact circularly polarized archimedean spiral antenna for ultrawideband communication applications," *IEEE Antennas and Wireless Propagation Letters*, vol. 16, pp. 129–132, 2017.

[20] M. Nosrati and N. Tavassolian, "Miniaturized circularly polarized square slot antenna with enhanced axial-ratio bandwidth using an antipodal Y-strip," *IEEE Antennas and Wireless Propagation Letters*, vol. 16, pp. 817–820, 2017.

[21] R. Natarajan, J. V. George, M. Kanagasabai, and A. K. Shrivastav, "A compact antipodal Vivaldi antenna for UWB applications," *IEEE Antennas and Wireless Propagation Letters*, vol. 14, pp. 1557–1560, 2015.

[22] S. X. Ta and I. Park, "Compact wideband circularly polarized patch antenna array using metasurface," *IEEE Antennas and Wireless Propagation Letters*, vol. 16, pp. 1932–1936, 2017.

[23] J. Bisharat, S. Liao, and Q. Xue, "Wideband unidirectional circularly polarized antenna with L-shaped radiator structure," *IEEE Antennas and Wireless Propagation Letters*, vol. 16, pp. 12–15, 2017.

[24] H. H. Tran and I. Park, "Compact wideband circularly polarised resonant cavity antenna using a single dielectric superstrate," *IET Microwaves, Antennas and Propagation*, vol. 10, no. 7, pp. 729–736, 2016.

[25] P. Sambandam, M. Kanagasabai, S. Ramadoss et al., "Compact monopole antenna backed with forkslotted EBG for wearable applications," *IEEE Antennas and Wireless Propagation Letters*, vol. 19, no. 2, pp. 228–232, 2020.

[26] M. Karimiyan-Mohammadabadi, M. Dorostkar, F. Shokuohi, M. Shanbeh, and A. Torkan, "Ultra-wideband textile antenna

with circular polarization for GPS applications and wireless body area networks," *Journal of Industrial Textiles*, vol. 46, no. 8, pp. 1684–1697, 2017.

[27] J. Kulkarni, A. G. Alharbi, C. Y. D. Sim et al., "Dual polarized, multiband four-port decagon shaped flexible MIMO antenna for next generation wireless applications," *IEEE Access*, vol. 10, pp. 128132–128150, 2022.

[28] J. Kulkarni, C.-Y.-D. Sim, R. Gangwar, and J. Anguera, "Broadband and compact circularly polarized MIMO antenna with concentric rings and oval slots for 5G application," *IEEE Access*, vol. 10, pp. 29925–29936, 2022.

[29] T. Addepalli, A. Desai, I. Elfergani et al., "8-port semi-circular arc MIMO antenna with an inverted L-strip loaded connected ground for UWB applications," *Electronics*, vol. 10, no. 12, p. 1476, 2021.

[30] N. P. Gupta, M. Kumar, and R. Maheshwari, "Development and performance analysis of conformal UWB wearable antenna under various bending radii," *IOP Conference Series: Materials Science and Engineering*, vol. 594, no. 1, article 012025, 2019.

[31] N. P. Gupta and M. Kumar, "Radiation performance improvement in wearable UWB antenna through slot insertion technique," in *2015 Fifth International Conference on Communication Systems and Network Technologies*, pp. 83–87, Gwalior, India, 2015.

[32] M. A. Antoniades, M. A. B. Abbasi, M. Nikolic, P. Vryonides, and S. Nikolaou, "Conformai wearable monopole antenna backed by a compact EBG structure for body area networks," in *2017 11th European Conference on Antennas and Propagation (EUCAP)*, pp. 164–166, Paris, France, 2017.

[33] V. Kumar and B. Gupta, "On-body measurements of SS-UWB patch antenna for WBAN applications," *AEU-International Journal of Electronics and Communications*, vol. 70, no. 5, pp. 668–675, 2016.

[34] R. Singh, D. Seth, S. Rawat, and K. Ray, "Performance investigations of multi-resonance microstrip patch antenna for wearable applications," in *Soft Computing: Theories and Applications*, K. Ray, T. Sharma, S. Rawat, R. Saini, and A. Bandyopadhyay, Eds., vol. 742 of Advances in Intelligent Systems and Computing, Springer, Singapore, 2019.

[35] A. Balanis, Ed., *Modern Antenna Handbook*, John Wiley & Sons, 2011.

[36] S. N. Mahmood, A. J. Ishak, T. Saeidi et al., "Full ground ultra-wideband wearable textile antenna for breast cancer and wireless body area network applications," *Micromachines*, vol. 12, no. 3, p. 322, 2021.

[37] P. Kumar, T. Ali, and A. Sharma, "Flexible substrate based printed wearable antennas for wireless body area networks medical applications (review)," *Radioelectronics and Communications Systems*, vol. 64, no. 7, pp. 337–350, 2021.

[38] I. U. Din, S. Ullah, S. I. Naqvi et al., "Improvement in the gain of UWB antenna for GPR applications by using frequency-selective surface," *International Journal of Antennas and Propagation*, vol. 2022, Article ID 2002552, 12 pages, 2022.

[39] P. Kumar and J. L. Masa, "Dual polarized monopole patch antennas for UWB applications with elimination of WLAN signals," *Advanced Electromagnetics*, vol. 5, no. 1, pp. 46–52, 2016.

[40] Z. Wang, M. Wang, and W. Nie, "A monopole UWB antenna for WIFI 7/bluetooth and satellite communication," *Symmetry*, vol. 14, no. 9, p. 1929, 2022.

[41] M. K. Verma, B. K. Kanaujia, J. P. Saini, and P. Saini, "A novel circularly polarized gap-coupled wideband antenna with DGS for X/Kuband applications," *Electromagnetics*, vol. 39, no. 3, pp. 186–197, 2019.

[42] U. Banerjee, A. Karmakar, A. Saha, and P. Chakraborty, "A CPW-fed compact monopole antenna with defected ground structure and modified parasitic hilbert strip having wideband circular polarization," *AEU-International Journal of Electronics and Communications*, vol. 110, article 152831, 2019.

[43] A. Laxman Kumar, A. Ranjan, M. Chauhan, V. K. Killamsetty, and B. Mukherjee, "Circular SRR shaped UWB antenna with WiMAX band notch characteristics," in *2018 IEEE Radio and Antenna Days of the Indian Ocean (RADIO)*, pp. 1-2, Wolmar, Mauritius, 2018.